A three-dimensional kinematic model for the deformation above an active diapir

Hongwei Yin and Richard H. Groshong Jr.

ABSTRACT

This article presents the results of a finite-thickness, three-dimensional (3-D) kinematic model for the fault-related deformation above an active diapir. Based on field examples, the models are (1) circular in map view; (2) offset by radially distributed normal faults; (3) faulted or smooth at the top of the salt; (4) relatively unstrained on the flanks; and (5) highly deformed in the central graben, if present. Field examples suggest that active diapirs may initiate with either two or three master faults crossing near the dome crest. Subsequent evolution depends mainly on whether the master faults cut the salt or detach on the salt top. If the top of the salt is faulted, no minor faults are required except in the central graben. If the top of the salt is unfaulted, additional faulting occurs in the flank grabens. In models with three master faults, very different structural patterns appear in cross sections cut parallel and perpendicular to any of the master faults. The domes are asymmetrical in the fault-perpendicular cross sections, but are symmetrical in the fault-parallel cross sections. The initial fault pattern may influence the piercement efficiency. An active dome with faults offsetting the top of the salt grows more rapidly than a dome with a smooth top and may develop into a passive diapir more rapidly. The model map patterns are used to reinterpret the 3-D structure of the Clay Creek dome, Texas, and the Reitbrook dome, Germany. The model predictions are confirmed by the cross sections, and small, but potentially significant, refinements are proposed.

INTRODUCTION

Salt domes and salt diapirs have long been important hydrocarbon-producing structures (e.g., Halbouty, 1967; Braunstein and O'Brien, 1968, and references therein), and new discoveries continue to be made around the world, for example, the Main Pass 299 field (Eisenberg and Dixon, 1999), the Lena field (Johnston et al., 2001),

Manuscript received April 10, 2006; provisional acceptance June 7, 2006; revised manuscript received August 27, 2006; final acceptance October 24, 2006.
DOI:10.1306/10240606034

AUTHORS

HONGWEI YIN ~ *Department of Earth Sciences, Nanjing University, Nanjing 210093, People's Republic of China; hwyin@nju.edu.cn*

Hongwei Yin is an associate professor of structural geology at Nanjing University, People's Republic of China, where he conducts research and teaches in the areas of quantitative structural geology and salt tectonics. He earned a B.S. degree (1993), an M.S. degree in geology (1996) from Nanjing University, People's Republic of China, and a Ph.D. in geology (2003) from the University of Alabama.

RICHARD H. GROSHONG JR. ~ *Department of Geological Sciences, University of Alabama, Tuscaloosa, Alabama 35487; rhgroshong@cs.com*

Richard H. Groshong, Jr., is an instructor for PetroSkills, Inc., and a professor emeritus at the University of Alabama. He has been chairman of the Structure and Tectonics Division of the Geological Society of America and an AAPG Distinguished Lecturer. He holds a B.S. degree from Bucknell University of Texas at Austin and a Ph.D. from Brown University.

ACKNOWLEDGEMENTS

The authors thank Alan Gibbs and Midland Valley Exploration, Ltd., for the use of the software 3DMove, John Spang at Texas A&M University for providing a copy of McDowell's thesis on the Clay Creek dome, and J. Schmitz for bringing the latest work on the Reitbrook dome to our attention and for providing additional data. This research has been supported in part by the U.S. Department of Energy Grant DE-FC02-91ER75678 and Contract DE-FC26-00NT40927, the National Natural Science Foundation of China Contract No. 40402019, and by a Graduate Council Fellowship from the University of Alabama to H. Yin. R. H. Groshong is grateful for support from Jiafu Qi, the director of the Key Laboratory for Hydrocarbon Accumulation Mechanism, China Petroleum University, People's Republic of China; National Natural Science Foundation of China Contract No. 40372072; and Ministry of Education Contract No. 200303. We thank Michael R. Hudec, Ronald A. Nelson, Sandro Serra, and Martha Withjack for their valuable reviews.

the Minden, Whitehouse, and Dry Creek domes (Turner et al., 2001) in the Gulf of Mexico, Kotyrtas North and Novobogatinsk fields in the Caspian Sea (Volozh et al., 2003), and the Tarim Basin, China (Tang et al., 2004). Even in the era of three-dimensional (3-D) seismic data, interpreting the structure in a dome or around a diapir remains challenging. As Davison et al. (2000a) observed, ''These reservoirs present a challenge to effective recovery of the hydrocarbons, as the seismic imaging of the reservoirs close to the diapirs is poor due to a combination of steeply dipping beds, intensely faulted strata, overlying gas clouds, extreme stratigraphic thickness changes, and poor velocity control.'' The fault patterns in the brittle cover over domes are typically complex because of the strongly 3-D nature of the deformation around the circular to elliptical structures that are the focus of this article. Interpretations based on well logs are also challenging because all faults tend to look alike, making the correlation of fault cuts into faults nonunique.

Adding to the difficulty of interpreting the faults around a diapir is the lack of generally accepted rules for the geometry and evolution of faults in 3-D. In the absence of a regional stress field, geoscientists widely recognize that the typical map pattern consists of normal faults with approximately radial map traces (Parker and MacDowell, 1951, 1955; Cloos, 1955; Halbouty, 1967; Withjack, 1979; Withjack and Scheiner, 1982; Fails, 1990; Schultz-Ela et al., 1993; Yin and Groshong, 2003). Dome fault patterns may also be caused or affected by vertical subsidence, either solution collapse (Christiansen, 1971; Gendzwill and Hajnal, 1971; Ge and Jackson, 1998; Clark et al., 1999) or extensional collapse (reactive domes; Vendeville and Jackson 1992; Jackson and Vendeville, 1994). We have found that when different investigators examine the same dome-related fault patterns, including those in this article, they may reach completely opposite conclusions as to the validity of the pattern and its mode of origin, emphasizing the need for generally acceptable validation techniques. Bed-length restoration is a successful validation tool when applied to two-dimensional structures like the elongate anticlines that form under regional extension or compression (Hossack, 1995), but has significant pitfalls when applied to faulted domal structures (Yin and Groshong, 2006). Map restoration (e.g., Yin and Groshong, 2006) is another appropriate validation tool, but applies to separate marker beds, not faulted 3-D volumes. Here, we examine the constraints on the fault patterns in a salt dome that are provided by volume-balanced, 3-D kinematic models for the origin and growth of a dome in which as much of the deformation as possible is accommodated by fault slip. The models are based on well-documented published examples, which are used to select the fault configurations to be tested. A valid 3-D fault array allows domal uplift, fault slip, and bed rotation, while at the same time maintaining the continuity of the dome across the faults. The models are allowed to deform to the point of incipient piercement to show the effects of increasing uplift and fault displacement on the fault pattern. The models have finite thickness, so that the 3-D geometry of the faults can be documented. We model active salt domes without significant influence of regional tectonics. We do not suggest that the models presented here represent all possible valid domal fault systems; only that they represent a kinematically valid suite of faulted-dome styles associated with uplift and arching. The insights gained from the models should help define this structural style in 3-D and help in the interpretation of poorly imaged dome-related fault patterns.

A salt (or shale) dome becomes a diapir when it pierces or partially pierces its overburden strata. Diapirs can pierce their overburden strata in three ways: actively (Nettleton, 1934, 1943; Gussow, 1968; Schultz-Ela et al., 1993), passively (Barton, 1933; Jackson and Talbot, 1991; Nelson, 1991; Rowan et al., 2003), and reactively (Vendeville and Jackson 1992; Jackson and Vendeville, 1994). An active diapir lifts and shoulders aside its roof (Vendeville and Jackson, 1992), a passive diapir remains at the depositional interface, whereas sediments are deposited around it (Barton, 1933; Vendeville and Jackson 1992), and a reactive diapir forms in regional extension as the isostatic response to thinning of the roof (Vendeville and Jackson 1992). Although the reactive and passive modes typically dominate the growth history of a diapir, radial fault patterns are almost certainly formed during active phases. Episodes of rapid deposition may bury the dome and be followed by new episodes of active diapirism (Jackson et al., 1988). Faults in passive intervals might inherit their pattern from the active phase. Thus, valid models for the active phase might also provide a guide to some structures of the passive phase.

We begin by synthesizing the geometry and fault patterns of natural domes to determine the essential elements and variables that must be included in the kinematic models. The effects of the variables on the final geometry are then illustrated by a series of 3-D models presented in both map and cross section. As an example of the application of the models to the interpretation of subsurface data, we conclude with a critique of the

kinematic compatibility of the fault patterns in two of the best documented domes and with suggestions for changes that would improve the compatibility.

STRUCTURAL PROPERTIES OF ACTIVE DIAPIRS

The characteristic features of active piercement structures identified in 11 well-documented natural salt domes are summarized here. These features provide a basis for the kinematic model to follow.

Active Diapirs Are Circular or Elliptical in Map View

In map view, the typical active diapir is approximately circular or elliptical and 3–5 km (1.8–3.1 mi) across. The Clay Creek dome is nearly perfectly circular and about 4.5 km (2.8 mi) in diameter at the top of the Wilcox Formation (Figure 1a). The Reitbrook dome is nearly circular and about 4–5 km (2.5–3.1 mi) in diameter at the level of the base of the Tertiary (Figure 1b). Similar examples of circular-shaped active domes include the Bayou Bleu (Smith and Reeve, 1970), Tiger Shoal (Figure 1c), Sugarland (Grinstead, 1962), Spindletop (Ewing, 1986), Port Neches (Ewing, 1986), Orange (Ewing, 1986), Kings (Karges, 1975), and West Clara (Figure 1d).

Active Diapirs Rise above the Surrounding Area

Because of the upward intrusion of the salt, strata above active diapirs are always above the regional elevations of coeval strata in the surrounding area (Figure 2). The crest of Clay Creek dome is approximately 800 m (2600 ft) higher than the surrounding area (Figure 1a). The Reitbrook dome has a crest about 500 m (1640 ft) higher than its surroundings (Figure 1b). The Orange, Port Neches, and Spindletop domes are about 300 m (1000 ft) higher than the regional elevation (Figure 2). As illustrated in Figures 1 and 2, the bedding over active domes dips radially away from the crest.

The Overburden Strata above Active Diapirs Are Ruptured by Radial Normal Faults

Radially distributed normal faults are common in the overburden strata above active domes. Typically, these faults are limited to the arched area of the overburden strata. Throw on these faults increases toward the crest and goes to zero at the edge of the dome. The Clay Creek dome (Figure 1a) is an active salt dome with a nearly ideal radial normal-fault pattern. The Tiger Shoal (Figure 1c) and West Clara domes (Figure 1d) also contain roughly radial fault patterns. The normal faults clearly exhibit a radial pattern in the northwestern area of the Reitbrook dome (Figure 1b). In the southeastern area, the radial pattern of faults is not as clearly developed because of the influence of minor faults. Several investigators, including Link (1930), Parker and MacDowell (1951, 1955), Cloos (1955), and Withjack and Scheiner (1982), have reproduced the radial normal faults associated with active diapirism in physical experiments.

Active Domes Have Few Faults in the Early Stage, and Many Faults in the Late Stage

Tiger Shoal and West Clara are gently dipping domes with crests about 100–200 m (330–660 ft) above the surrounding area (Figure 1c, d). The flanks of the Clay Creek and Reitbrook domes are relatively steeply dipping, and their crests are about 500–800 m (1640–2600 ft) above the surrounding area (Figure 1a, b). Low relief and gentle dip of the overburden strata in the Tiger Shoal and West Clara domes imply that they are early-stage domes, whereas relatively high relief and steep dip of the overburden strata in the Clay Creek and Reitbrook domes show that they are in a later stage of development. The Tiger Shoal and West Clara domes have few normal faults, whereas the Clay Creek and Reitbrook domes have many normal faults (Figure 1). Both the Tiger Shoal dome and the West Clara dome have two long normal faults, which go through the dome and cross each other near the dome crest. We interpret such long faults that go through the dome as the master faults initiated during the very early stage of the dome growth (Figure 3). The master faults have maximum throw near the crest. Fault displacement decreases to zero away from the crest. Late-stage domes like the Clay Creek and Reitbrook domes show a more complicated fault pattern with more faults. For both the Clay Creek dome and the Reitbrook dome, we pick three master faults (Figure 3). The master faults cross the dome and cross each other near the dome crest. One purpose of our research is to show the effects of increasing uplift and fault displacement on the fault pattern. We show in our forward modeling how an active salt dome with two or three initial master faults can develop more faults and a more complicated fault pattern with increasing uplift.

Based on the number of master faults and their arrangement, we name the fault patterns of active domes as resembling either an X or Y pattern. The X pattern

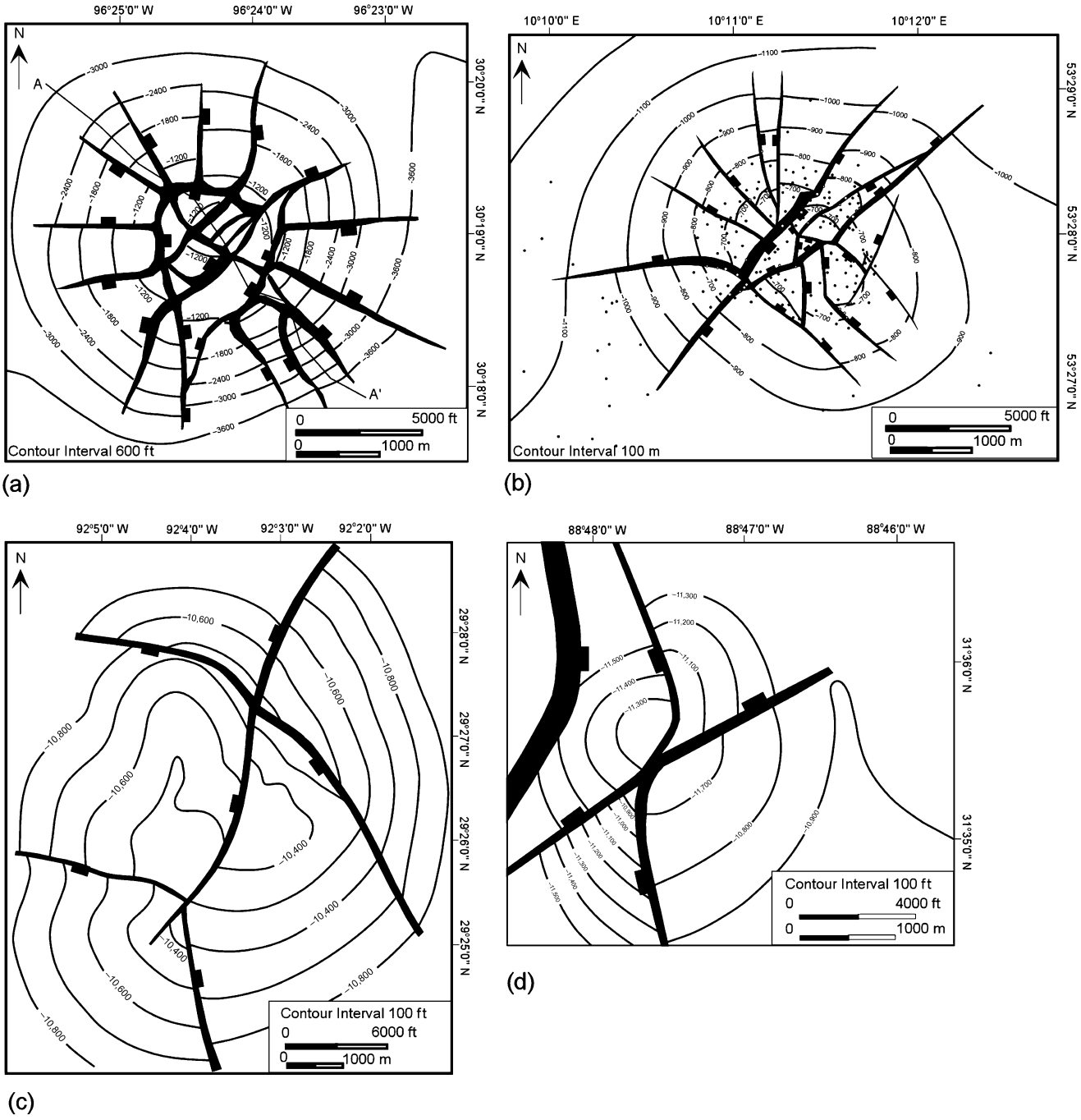

Figure 1. Structure contour maps of representative active salt domes. Latitudes and longitudes of maps in this and the following figures, except the Reitbrook dome, are derived from Lat-Long Services (2006). (a) Clay Creek dome, Texas, showing normal faults and contours on top of the Wilcox Formation (from McDowell, 1951). (b) Reitbrook dome, Germany, showing normal faults and contours on the base of the Tertiary (from Schmitz and Flixeder, 1993, with kind permission of Springer Science and Business Media). (c) Tiger Shoal dome, Louisiana, showing normal faults and contours on the top of T sand (from Smith et al., 1988; reprinted with permission from the New Orleans Geological Society). (d) West Clara dome, Mississippi, showing normal faults and contours on the base of the Ferry Lake anhydrite (from Davis and Lambert, 1963; reprinted with permission from the Mississippi Geological Society).

represents active diapirism beginning with two master normal faults. The two faults cut the dome into four blocks, one horst, one graben, and two half grabens. The West Clara dome and the Tiger Shoal dome (Figure 3a, b) are examples of this pattern. No central graben is observed in domes with only two master normal faults. The

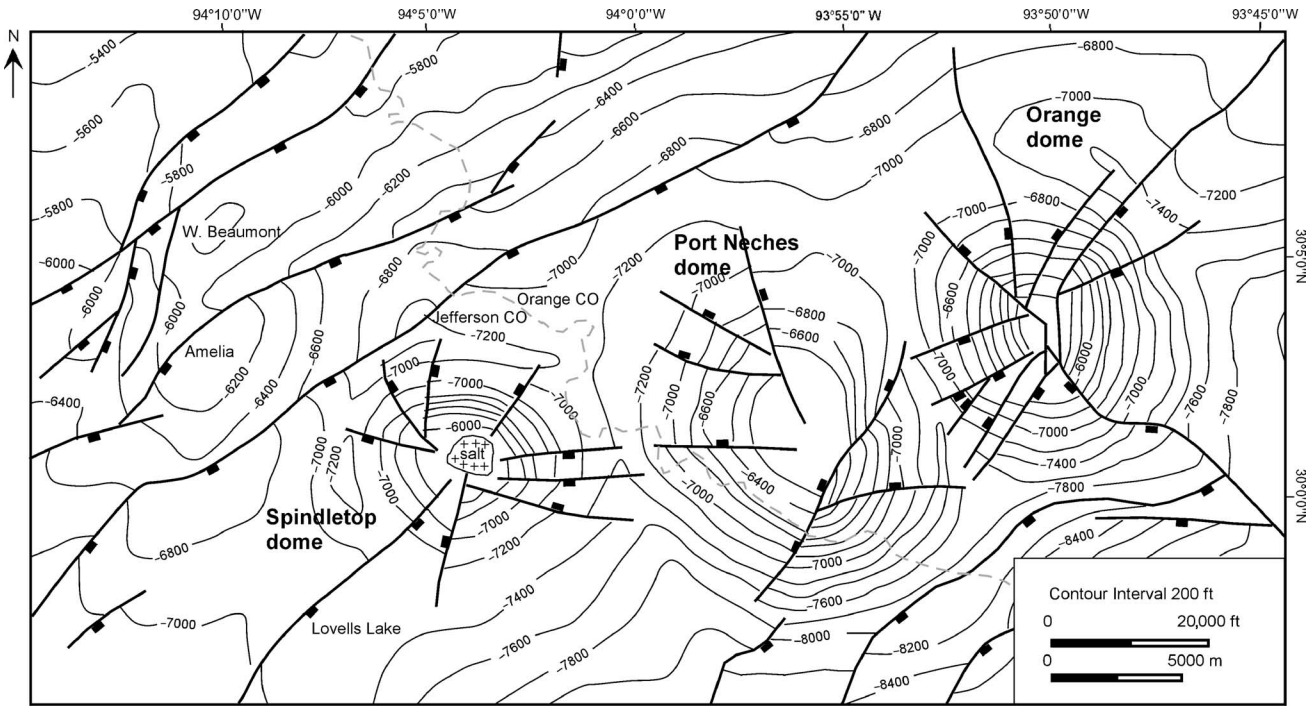

Figure 2. Structure contour map on A2 horizon, Port Arthur area, Texas (modified from Ewing, 1986).

Y pattern represents active diapirism beginning with three master faults. The Reitbrook and Clay Creek domes are affected by Y-pattern master faults (Figure 3c, d). The three master faults in the Reitbrook dome are asymmetrical, defining one horst block, one graben block, and three half-graben blocks. One minor fault near the crest of the dome separates the tip of the graben from the rest of the block and forms a wedge-shaped central graben (Figure 3d). The three master faults in the Clay Creek dome are radially symmetrical and cut the dome into three horst blocks, three graben blocks, and a highly fractured and thinned triangular central graben (Figure 3c). The grabens of the Clay Creek dome and the half grabens in the Reitbrook dome are further deformed by minor normal faults. In both the X and Y styles, almost all the faults are limited to the arched dome area, and minor faults always terminate against master faults or other minor faults.

The Overburden Strata on the Dome Flanks Are Relatively Unstrained

Rocks deformed under low temperature typically show only small internal strains between faults (Groshong, 1988). Physical and numerical models by Schultz-Ela et al. (1993) show that the strain of active diapirism is typically concentrated in the central graben, and that the flank flaps, which deform by rotating upward and outward, are relatively unstrained. Brewer and Groshong (1993) constructed models to simulate the uplift of flank strata and produced low, broad uplifts with relatively undeformed flanks and a highly deformed central graben. Evidence of relatively unstrained flanks and a highly deformed central graben can be interpreted from the cross section of the Bayou Bleu dome (Figure 4). The flanks of the dome have been tilted and elevated above the regional elevation. The thickness change in the *Siphonina davisi* sandstone and the interval from P to O is very small across the dome. The constant thickness of these intervals shows that appreciable strain-related internal thickness changes are not required by the doming process even at the crest. However, Davison et al. (2000b) have made direct observations on cores from domes in the Central Graben of the North Sea and found substantial tectonic thinning. Where thickness changes on the flanks of domes occur, they may be caused by either syntectonic sedimentation or internal deformation. We model constant-thickness beds as a base case.

Top of Salt May Be Smooth or Faulted

The top of the salt on some domes appears to be continuous and smooth, e.g., the Eugene Island Block 175 field (Figure 5a) and the West Bay dome (Figure 5b) in southern Louisiana. The smooth salt top has the shape of a hemisphere with a contour pattern composed of a

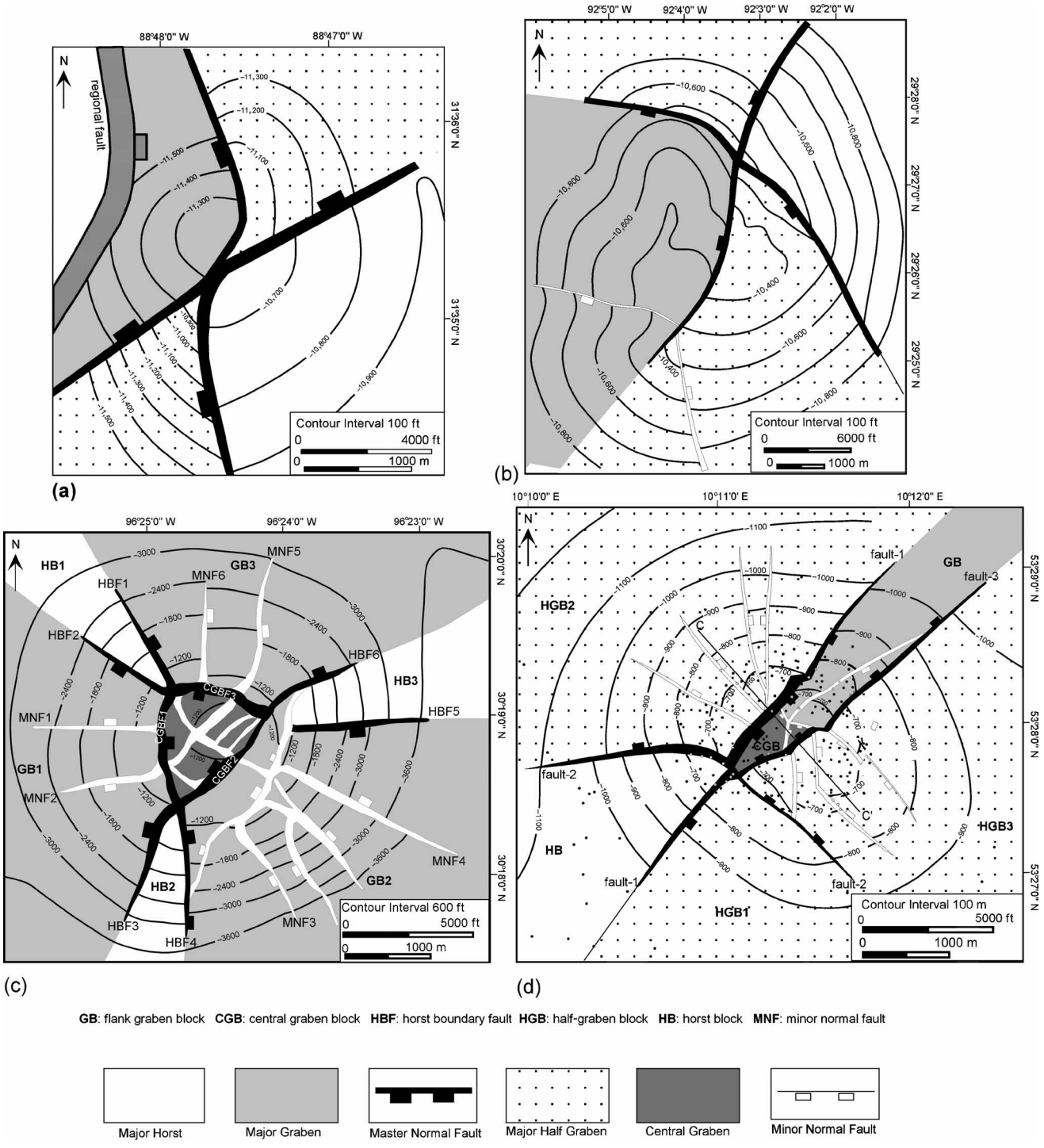

Figure 3. Characteristic fault map patterns of circular domes. (a) X pattern, structure contour map of West Clara dome, Mississippi, drawn on the base of the Ferry Lake anhydrite (from Davis and Lambert, 1963; reprinted with permission from the Mississippi Geological Society). (b) X pattern, structure contour map of Tiger Shoal dome, Louisiana, drawn on top of the T sand (from Smith et al., 1988; reprinted with permission from the New Orleans Geological Society). (c) Symmetrical Y pattern, structure contour map of Clay Creek dome, Texas, drawn on top of the Wilcox Formation (from McDowell, 1951). (d) Asymmetrical Y pattern, structure contour map of Reitbrook dome, Germany, drawn on the base of the Tertiary (from Schmitz and Flixeder, 1993 with kind permission of Springer Science and Business Media).

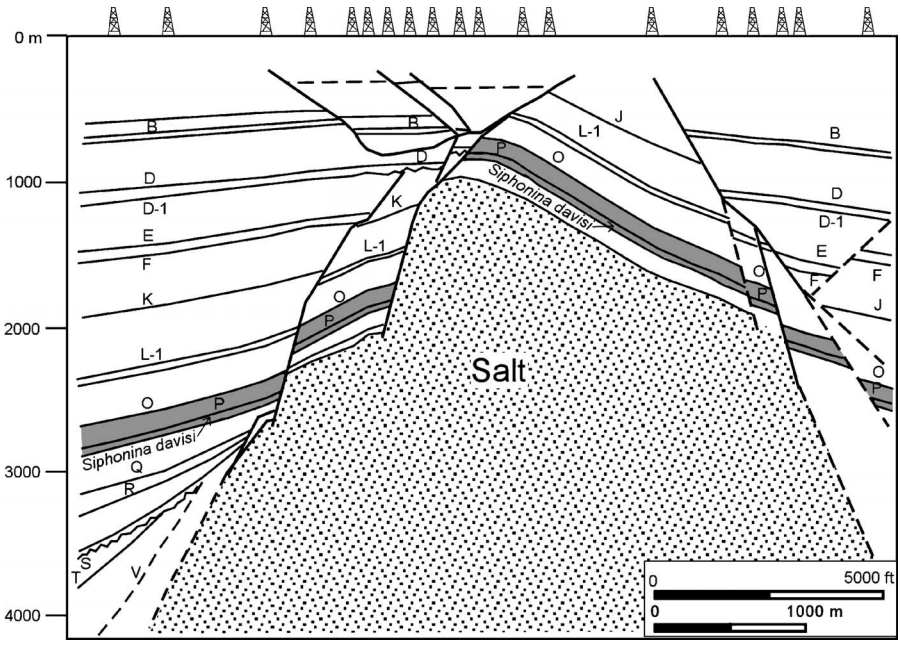

Figure 4. Cross section through Bayou Bleu field, southern Louisiana (from Smith and Reeve, 1970; reprinted with permission from AAPG). The *Siphonina davisi* bed and the interval from P to O (shaded units) maintain constant thickness.

series of concentric circles (Figure 5a, b). In the domes with a smooth salt top, faults must die out at or sole into the top of the salt (Figure 5c), and the top of the salt is the lower detachment for the overburden strata.

Salt can fail in a brittle mode at shallow levels. For example, faults offset the Aptian halite and sylvinite in a salt dome mined near Aracaju, in the Sergipe-Alagoas Basin of Brazil (Davison et al., 1996). The top of the salt in the Bayou Bleu field (Figure 4) is faulted. The contour map of a faulted salt top shows roughly concentric contour lines that are distorted by numerous indentations (Figure 6a, b). In the Bryan Mound dome, the position of the salt top indentations (Figure 6b) matches with faults in the overburden strata (Figure 6c).

KINEMATIC MODEL

Based on the essential features of active salt domes discussed in the section above, our 3-D kinematic model has the following characteristics. (1) The dome is circular in map view. (2) Domes initiate with two or three crossing master normal faults in the overburden strata. (3) Faults may sole into the top of the salt, or they may offset the upper part of the salt. (4) The flanks of the dome are relatively unstrained and keep constant map area and constant thickness as much as possible. (5) Deformation in the dome flanks is mainly by slip along faults. (6) The central graben is highly deformed but remains constant in volume.

We first consider Y-pattern models having three radially symmetrical master faults that cross at the crest of the dome (e.g., Figure 3c). Then, we extend the kinematic models to include the asymmetric Y-pattern (Figure 3d) and the X-pattern models (Figure 3a, b). In the Y-pattern model, three radially symmetrical master normal faults cut the dome into three horsts, three flank grabens, and a triangular-shaped central graben (Figure 7a). A hinge line separates the dipping dome area from the horizontal regional elevation. The upward movement of the salt causes the horsts and flank grabens to rotate upward and radially outward. The flank rotation is modeled by layer-parallel flexural slip, a kinematic mechanism that allows the preservation of the map area and bed thickness of each block. The layer-parallel flexural slip is radial to the dome along the centerline of each block, which preserves a constant length for each surface along the centerline (e.g., c1–c6 in Figure 7). The lengths of the concentric arcs perpendicular to the centerline are also preserved (e.g., a1c1b1–a5c5b5 in Figure 7), so the area is preserved. The central graben of the model domes is highly deformed. Instead of attempting to model the large number of small faults that must form in the central graben, we treat this part of the dome as a region of homogeneous strain with constant volume.

Both the faulted and smooth top of the salt will be considered. We assume that horst and graben blocks remain in contact across faults as long as this remains physically possible. If the top of the salt is faulted, the horst will have a steeper dip than the flank graben. Taking the

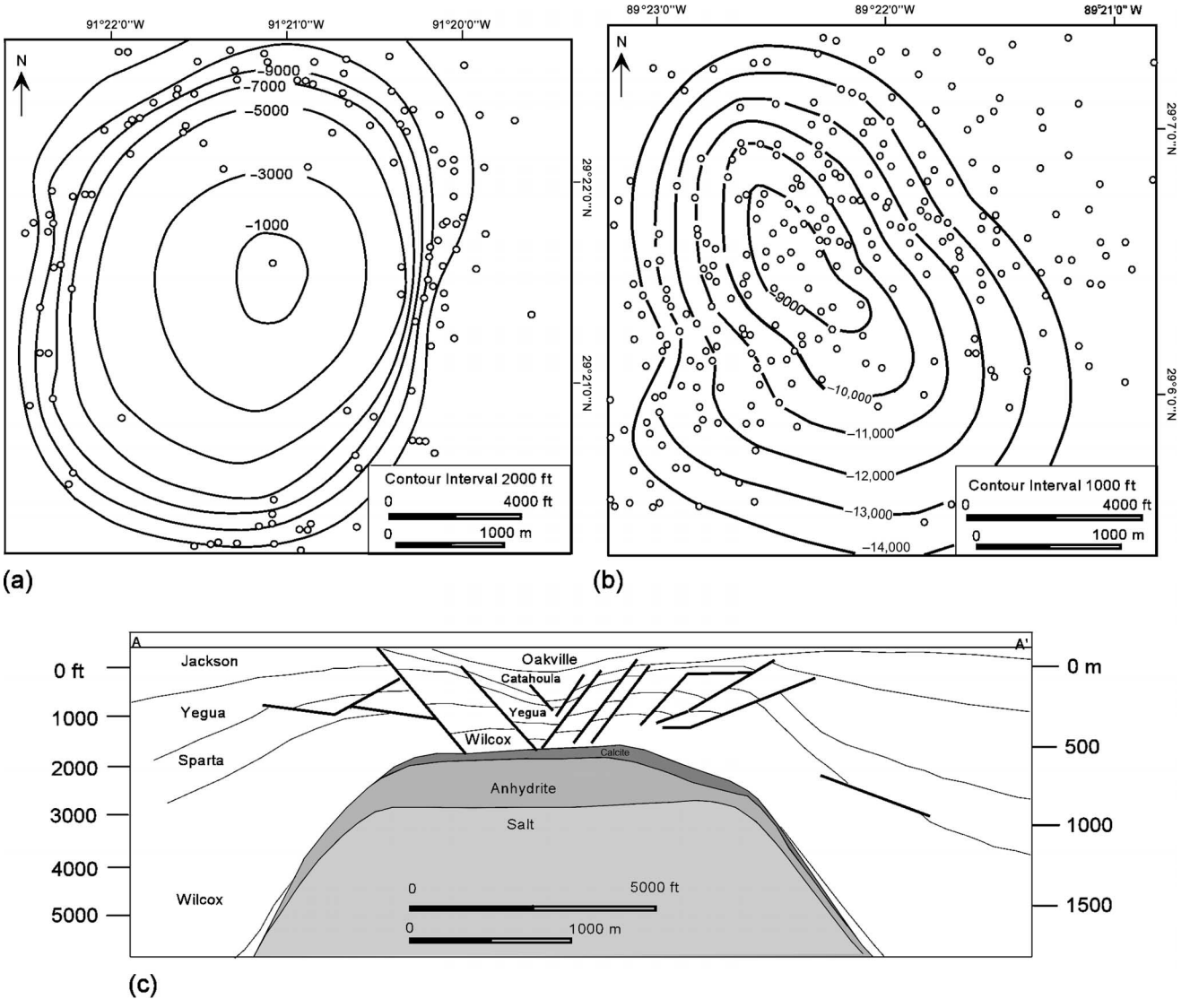

Figure 5. Domes with a smooth top of salt. (a) Map of Eugene Island Block 175 field, Louisiana, showing contours on top of the salt (from Waguespack, 1983; reprinted with permission from the New Orleans Geological Society). (b) Map of the West Bay dome, Louisiana, showing contours on top of the salt (from Waguespack, 1983; reprinted with permission from the New Orleans Geological Society). (c) Cross section of Clay Creek dome, Texas (from McDowell, 1951). The location is given in Figure 1a.

dip of the horst as the independent variable, the kinematic model is used to find the dip of the flank graben based on the minimization of the gap and overlap space where the graben and horst are in contact across a fault (Figure 8). If the top of the salt is smooth, the horst and flank grabens rotate the same amount. Hence, the dip of the flank grabens must equal the dip of the horsts after block rotation (Figure 9a). Wide gaps result between the horsts and grabens (Figure 9a), showing that the flank grabens must be further deformed. We use vertical simple shear in the smooth-salt-top models to further deform the flank grabens to close the gap between the adjacent horst and graben blocks (Figure 9b). With slight modifications, this model applies to the salt domes with the X pattern and asymmetrical Y pattern (Figure 3). Yin (2003) provides a detailed discussion of the modeling procedures.

GEOLOGIC INSIGHTS FROM 3-D KINEMATIC MODELS

Structural Styles of Circular Domes Expressed in Map View

Master faults in the overburden strata of active diapirs cross each other near the crest of the dome (Figure 3). To maintain symmetry and physical continuity, the

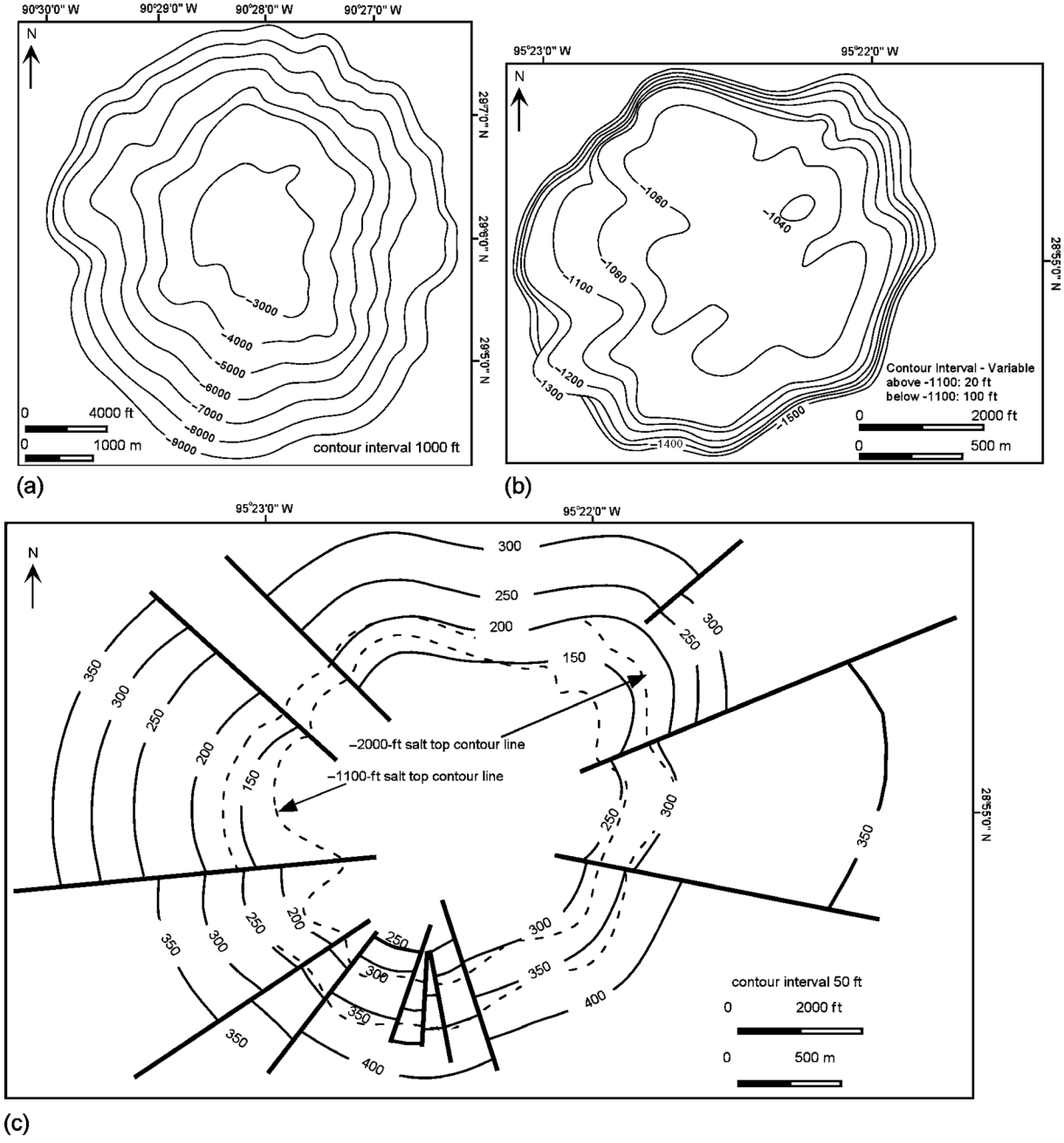

Figure 6. Domes with faulted top of salt. (a) Map of Caillou Island dome, Louisiana, showing contours on top of the salt (from Waguespack, 1983; reprinted with permission from the New Orleans Geological Society). (b) Map of Bryan Mound dome, Texas, showing contours on top of the salt (from Looff and Looff, 1999; reprinted with permission from the Gulf Coast Association of Geological Societies). (c) Map of Bryan Mound dome, Texas, showing the interval C isopach map (from Looff and Looff, 1999; reprinted with permission from the Gulf Coast Association of Geological Societies).

master faults move simultaneously and are mutually offsetting (Figures 10, 11). In the symmetrical Y-pattern model, each master fault is divided into three parts, the outer two of which act as horst boundary faults, and a central part acts as a boundary fault of the central graben (Figures 10a, 11a). In the model with two master faults, each major fault is divided into two parts, and each part acts as a boundary of the horst or the half graben (Figures 10b, 11b).

When master faults offset the top of the salt, no minor faults are developed in the horsts or flank grabens (Figure 10). When master faults do not cut the top of the

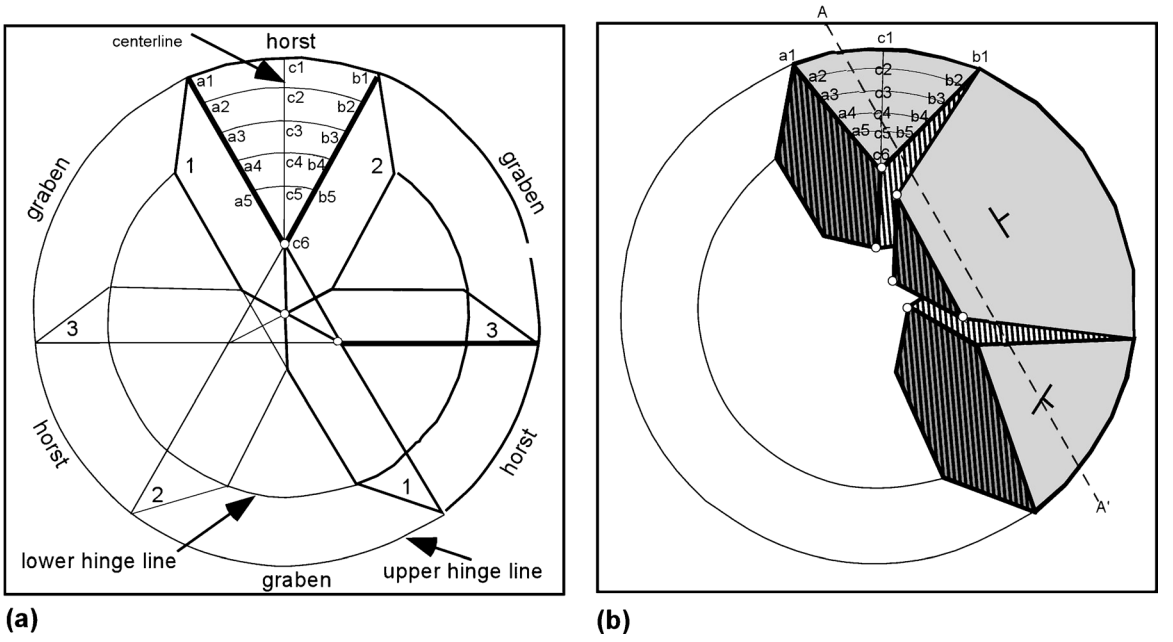

Figure 7. Fault geometry in the model having three radially symmetric master normal faults. (a) Before deformation. (b) After deformation.

salt, the central parts of the flank graben and half-graben blocks are relatively undeformed, although the sides of the flank grabens are deformed by vertical simple shear, forming troughs bounded on one side by a master fault and on the other by a highly strained region. These highly strained regions are likely to become secondary minor faults dipping toward the adjacent master fault. Each flank graben is likely to develop two minor faults, and each half graben is likely to develop one minor fault. In all the models, no minor faults are required in the horst blocks.

Structural Styles of Circular Domes Expressed in Cross Section

To investigate the expression of circular domes in cross section, we cut orthogonal serial sections from the model domes (Figures 12–16). In addition to the control on style exerted by the faulted or unfaulted nature of the salt top, the direction of the cross section is critical. The structural styles appear to be quite different in cross sections parallel and perpendicular to any of the master normal faults. The domes are symmetrical in sections parallel to a master fault (Figures 13, 15), but are asymmetrical in sections perpendicular to a master fault (Figures 14, 16). The structures in the perpendicular sections are more complex and variable than the structures in the parallel sections. Each parallel section has

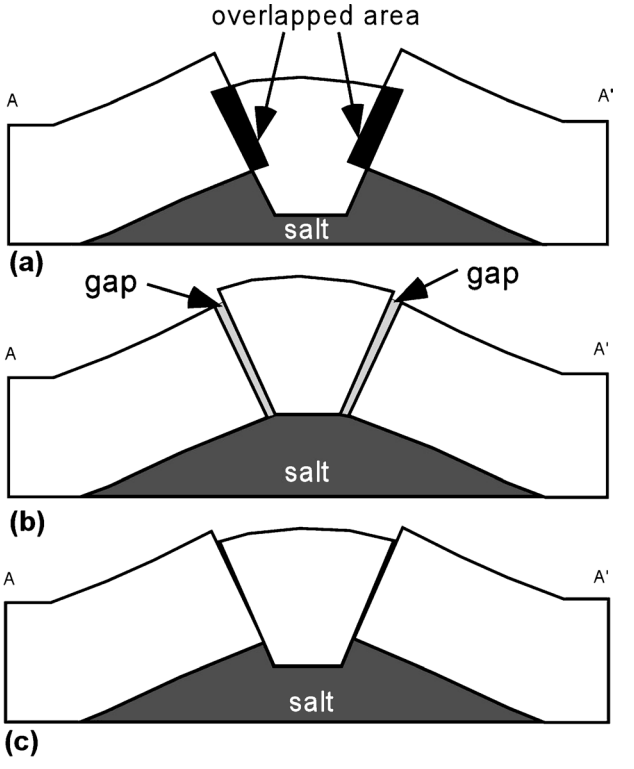

Figure 8. Cross section from model dome with faulted top of salt after 30° of horst-block rotation. Location given in Figure 7b. (a) Not enough uplift of the graben, the black regions adjacent to the faults indicate the overlapped area. (b) Too much uplift of the graben causes a gap. (c) Best fit between horst and graben blocks. The dip of the graben is 21.5°.

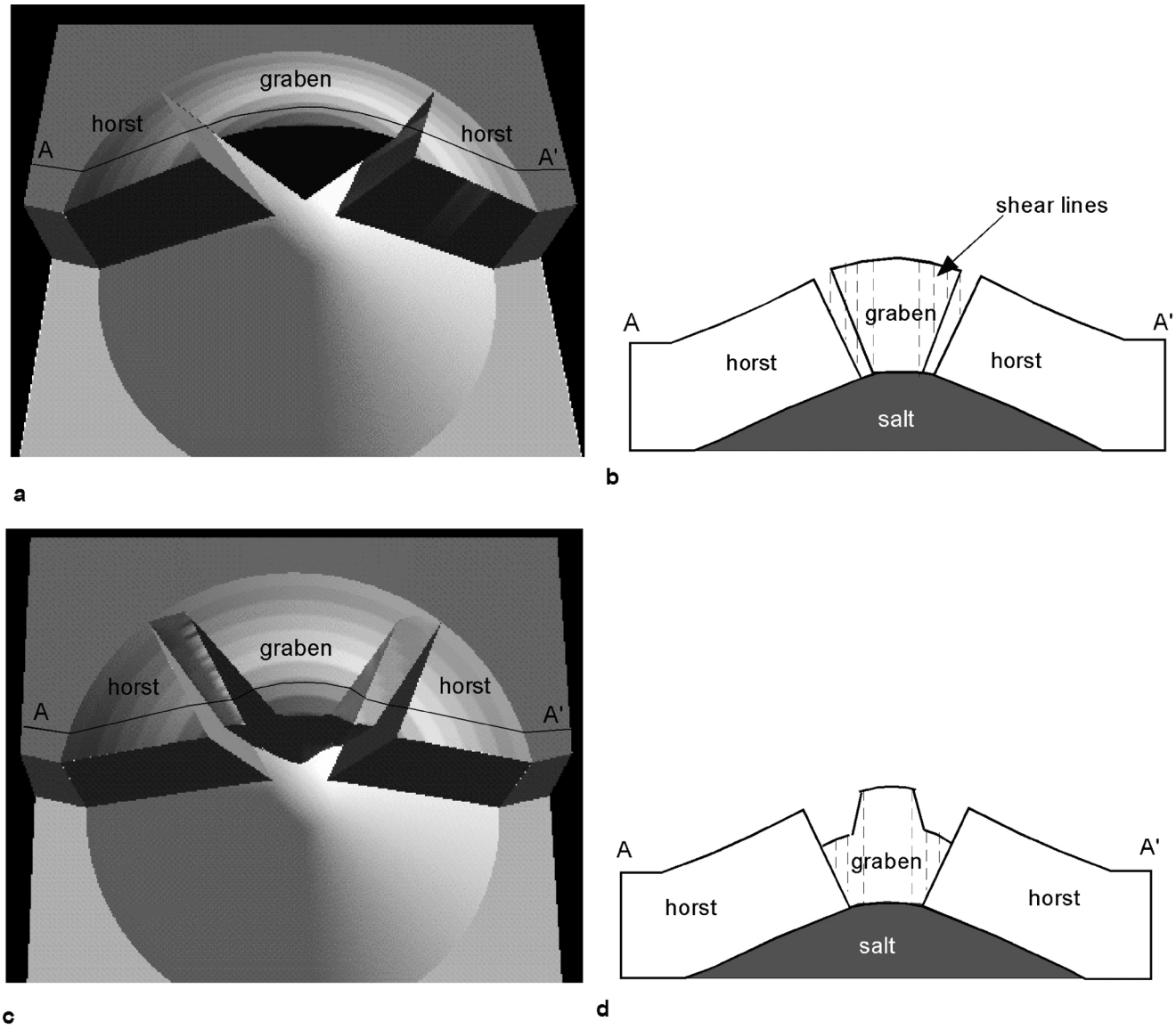

Figure 9. Model with unfaulted top of salt. The horst and graben blocks dip radially 30° away from the crest of the dome. (a) Initial configuration of the model. (b) Cross section from (a). (c) Model after closing the gap by vertical simple shear. (d) Cross section from (c).

two normal faults, which act as the boundary faults of a graben (Figures 13a, b; 15a, b) or a horst (Figures 13c, 15c). Each perpendicular section may contain one (Figures 14a, 16a), two (Figures 14b, d; 16c), or three (Figures 14c, 16b) normal faults. The perpendicular sections may include half grabens (Figures 14a, 16a), full grabens (Figures 14d, 16c), horsts (Figures 14b, c; 16c), or complicated horst and graben structures (Figure 16b).

In both parallel and perpendicular cross sections, the style of the cross section changes with the position of the section plane. On the fault-parallel sections, as the section plane moves from north to south (Figure 12), the style changes from a full graben that roughly maintains its original thickness in the center (Figures 13a, 15a), to a thinned (Figure 13b) or highly thinned central graben (Figure 15b), to a horst that roughly maintains its original thickness (Figures 13c, 15c). On fault-perpendicular sections, as the section plane moves from the outer edge to the center of the dome (Figure 12), the structural style changes from a half graben displaced by one master normal fault (Figures 14a, 16a), to a horst displaced by two master normal faults (Figure 14b), to a graben, or complex horst and graben structure displaced by all three major normal faults (Figures 14c, 16b), to a structure with constant bed-thickness flanks and a thinned, highly strained central graben (Figures 14d, 16c).

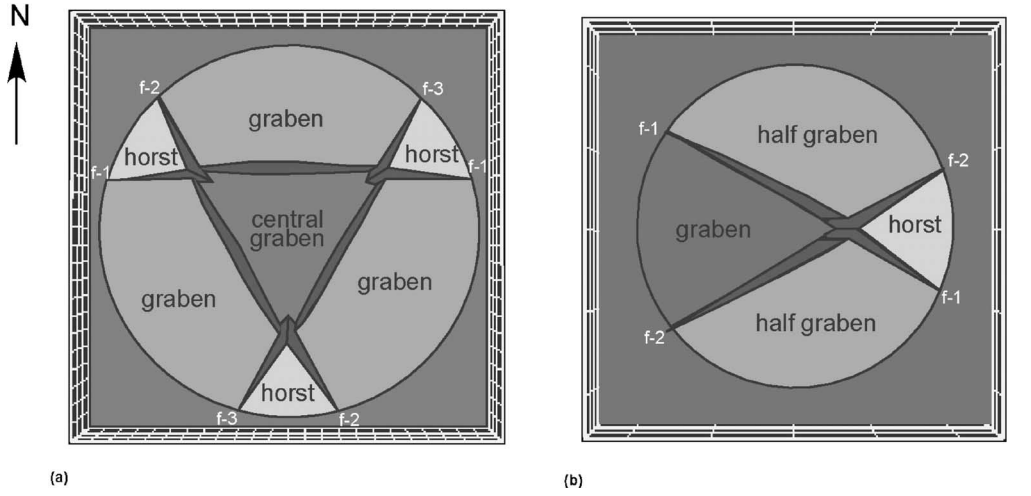

Figure 10. Models with a faulted top of salt. The horst blocks in each model dip 30° away from the crest of the dome. (a) Three radially symmetrical normal faults (Y pattern). (b) Two normal faults (X pattern).

The central graben always shows structural thinning because of the high subresolution strain and out-of-plane volume transport (Figures 13b, 15b, 16c).

Relationship between Fault Pattern and Dome Growth

We describe here the relationship between fault pattern and dome growth for symmetric Y-pattern dome models (Figure 17). All the model domes described in this section have a radius equal to 2.5 km (1.5 mi) on the bottom of the arched overburden strata. In both salt-top–faulted and salt-top–unfaulted models, the volume of salt in the dome increases during progressive uplift. The fault pattern exerts a significant influence on the dome growth. In the model with a faulted top of salt, when the dip of the horst increases from 10 to 50°, the volume of salt in the dome increases from 2.5 to 10.6 $\times$ 10^9 m^3 (0.88 to 3.74 $\times$ 10^{11} ft^3), a 324% increase. In the model with unfaulted top of salt, when the dip of the horst increases from 10 to 50°, the volume of the salt in the dome increases from 2.87 to 19.2 $\times$ 10^9 m^3 (1.01 to 6.78 $\times$ 10^{11} ft^3), a 569% increase. In other words, if the salt supply rate is the same, then a dome with faults offsetting the top of the salt might grow faster than a dome with a smooth top of the salt. This means that a dome with a faulted top of salt might be more quickly pierced and develop into a passive diapir than a dome with an unfaulted top of salt.

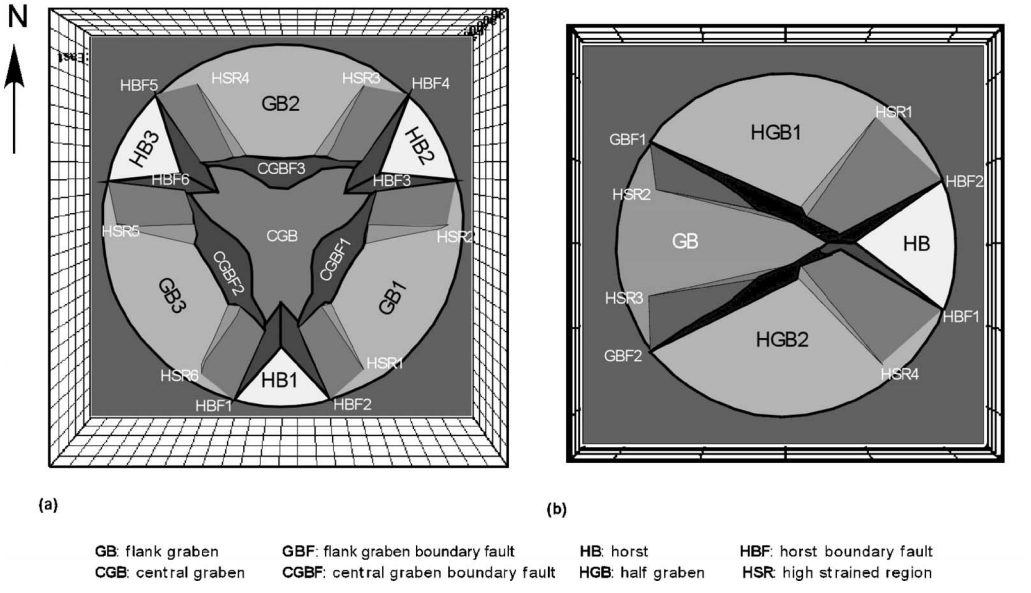

Figure 11. Models with unfaulted top of salt. (a) Three radially symmetrical normal faults (Y pattern). (b) Two normal faults (X pattern).

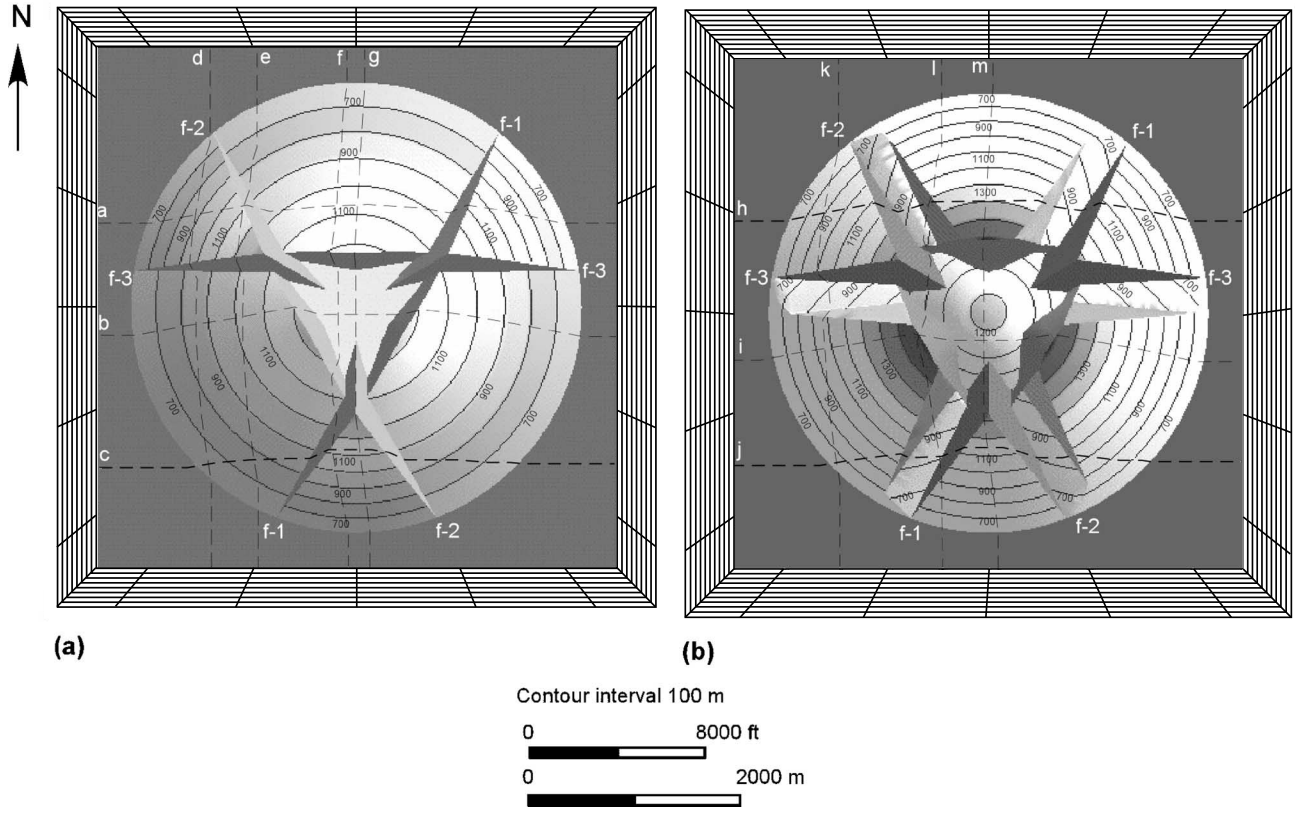

Figure 12. Symmetrical Y-pattern domes, with locations of cross sections. Master normal faults are f-1, f-2, and f-3. Letters a – m indicate the locations of cross sections in Figures 13 – 16. (a) Model dome with the faulted top of salt. (b) Model dome with the unfaulted top of salt.

APPLICATION OF MODEL RESULTS TO NATURAL EXAMPLES

The model results described above are used to critique the interpretations of the Clay Creek and Reitbrook domes and to suggest possible changes that would make the fault patterns more internally consistent.

The Clay Creek Dome

The Clay Creek dome (Figures 3c, 5c) is a typical faulted salt dome (Health et al., 1931; Ferguson and Minton, 1936; McDowell, 1951; Parker and MacDowell, 1951, 1955). McDowell (1951) provides the most complete interpretation. The three crossing master faults of this

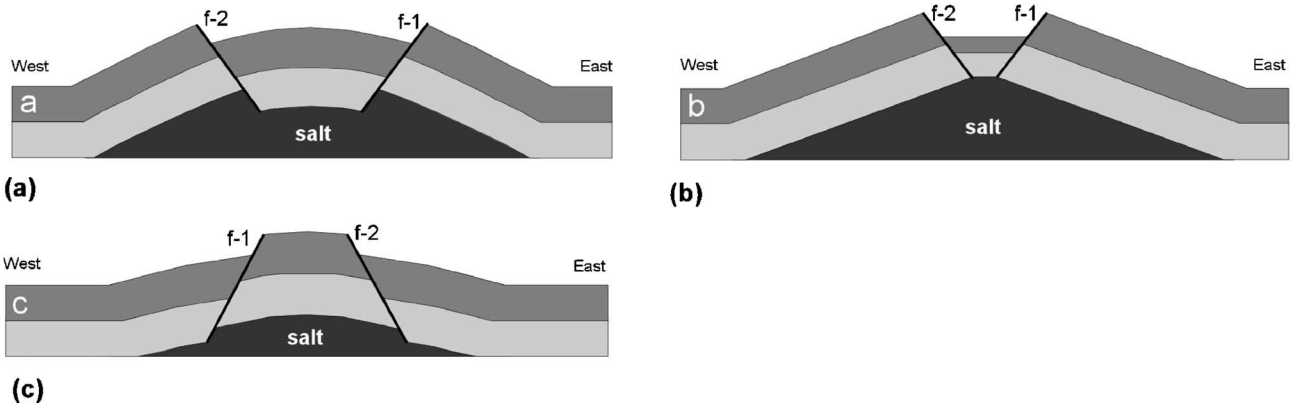

Figure 13. Cross sections parallel to a master normal fault in the Y-pattern dome with a faulted top of salt. Letters on the cross section correspond to the section lines in Figure 12a. (a) Section perpendicular to the centerline of the flank graben. (b) Section across the central graben. (c) Section perpendicular to the centerline of the flank horst.

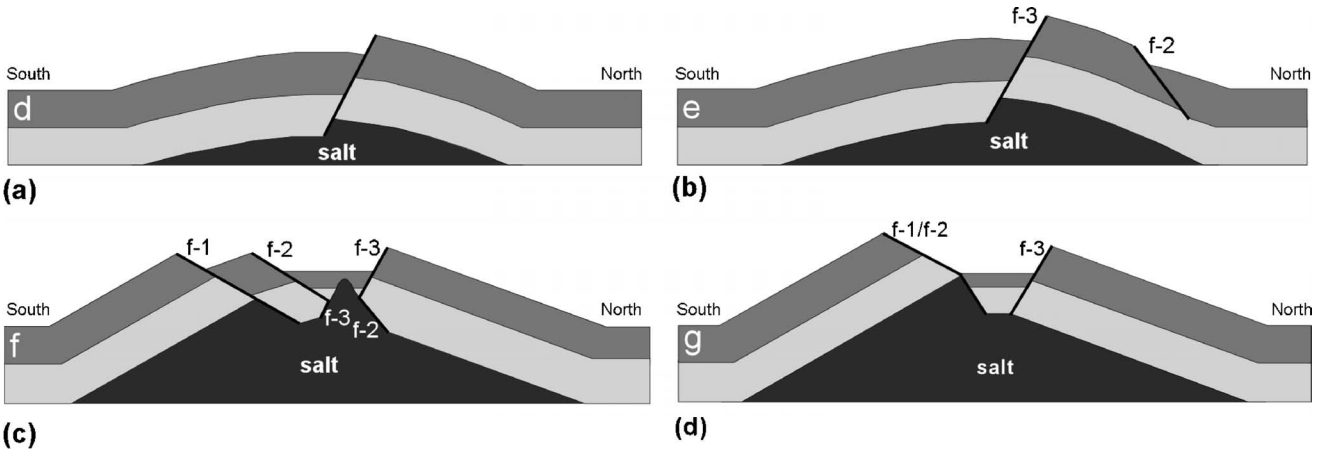

Figure 14. Cross sections perpendicular to a master normal fault in the Y-pattern dome with a faulted top of salt. Letters on the cross section correspond to the section lines in Figure 12a. (a) Section across one major normal fault. (b) Section across two major normal faults. (c) Section across all three major normal faults. (d) Section across the central graben along the centerline of the flank graben.

dome represent our type example of the symmetric Y-pattern dome. The minor fault geometry (Figure 3c) is comparable to the model dome with an unfaulted top of salt (Figure 11a). No minor faults are developed in the horsts where none are predicted. Flank grabens of the Clay Creek dome are deformed by minor normal faults, a feature characteristic of the model with unfaulted top of salt (Figure 11a). Flank grabens GB1 and GB3 (Figure 3c) each develop two minor faults, (1) MNF1 and MNF2 and (2) MNF5 and MNF6, respectively. The occurrence and position of these minor radial normal faults agree with the highly strained regions in the model, (1) HSR1 and HSR2 and (2) HSR5 and HSR6 (Figure 11a). The model dome predicts that the minor faults should be antithetic, dipping toward the adjacent horst boundary fault, as do the minor faults MNF1, MNF2 in graben GB1, and MNF5 in graben GB3 (Figure 3c). The middle parts of the major flank grabens have the same dip and elevation as the adjacent horst blocks, another characteristic feature of the unfaulted-salt model. Graben GB2 contains two antithetic faults for each master fault, indicating a wider zone of deformation than in the model. Had the model used a 60° antithetic simple shear instead of a vertical simple shear, the zone of hanging-wall deformation would have been wider and more likely to be accommodated by more than one fault. Shear angles ranging from vertical to about 60° antithetic are common in extensional structures (e.g., White et al., 1986; Rowan and Kligfield, 1989; Groshong, 1990, 2006).

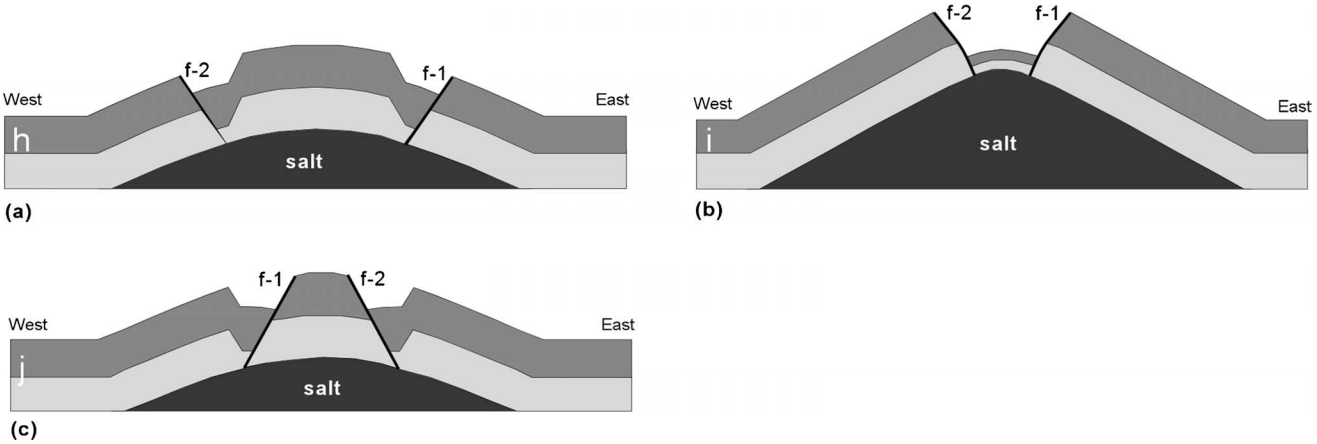

Figure 15. Cross sections parallel to a master normal fault in the Y-pattern dome with a smooth top of salt. Letters on the cross section correspond to the section line in Figure 12b. (a) Section perpendicular to the centerline of the flank graben. (b) Section across the central graben. (c) Section perpendicular to the centerline of the flank horst.

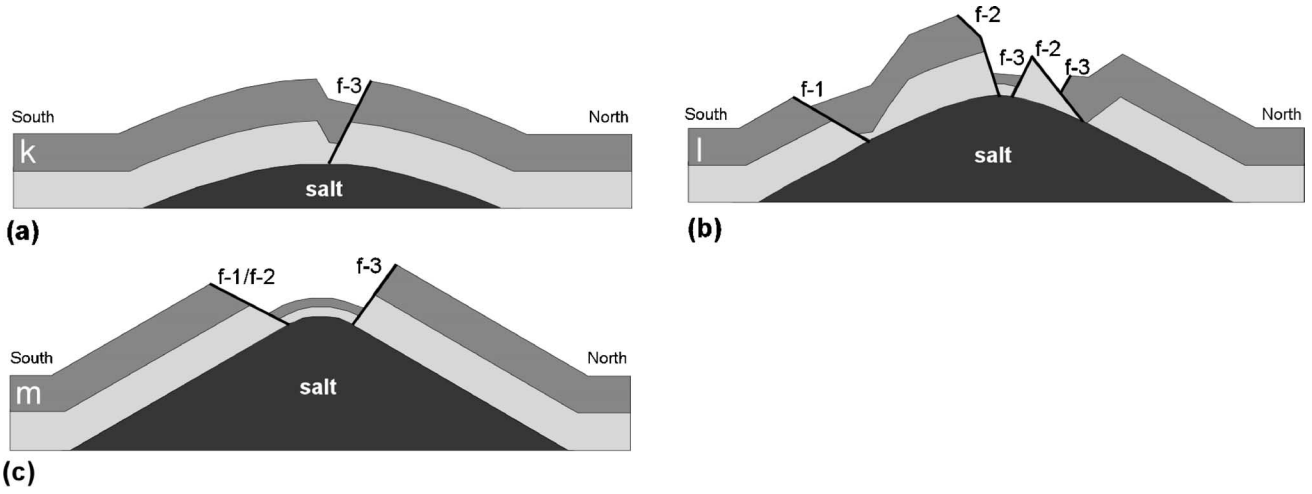

Figure 16. Cross sections perpendicular to a master normal fault in the Y-pattern dome with a smooth top of salt. Letters on the cross section correspond to the section line in Figure 12b. (a) Section across one major normal fault. (b) Section across two major normal faults. (c) Section across the central graben along the centerline of the flank graben.

In the Clay Creek dome, significant uplift occurred after the deposition of the Wilcox Formation (McDowell, 1951). The structure of the Wilcox Formation observed in cross section AA′ (Figure 5c) compares to the model section normal to a master fault and along the centerline of a flank graben (Figure 16c). As expected from the model, the central graben of the Clay Creek dome is greatly thinned by multiple small faults. In contrast to the model, units on the flanks of the Clay Creek dome increase in thickness away from the crest, indicating a deposition during deformation. The flank structure is simple as in the model.

The model results also give insight into potential problems and provide alternatives. The minor normal fault MNF6 in graben GB3 (Figure 3c) occurs in the location predicted by the model dome. However, instead of dipping toward the adjacent horst block boundary fault as predicted in the model dome, this fault dips away from it. This inconsistency implies either that it might be remapped and found to dip the opposite direction (Figure 18), or that it belongs to a wide deformed zone associated with master fault HBF6. A tangential normal fault complicates the southeast part of the dome. In the model, all the boundary faults of the horsts are segments of the master normal faults (Figure 11a). In the Clay Creek dome, all the horst-boundary faults are segments of the master normal faults, except fault HBF5. Faults HBF1, CGBF1, and HBF4 form one master normal fault. Faults HBF3, CGBF2, and HBF6 form another master normal fault. The third master normal fault predicted in the model should be composed of HBF2, CGBF3, and HBF5. However, instead of connecting to CGBF3 and working as one segment of a master normal fault, fault HBF5 terminates against the tangential fault. As an alternative, fault HBF5 could connect to CGBF and truncate the tangential fault (Figure 18). The revised map (Figure 18) agrees with the model and restores better with smaller overlap and gap areas than does the map in the original (Yin and Groshong, 2006).

The Reitbrook Dome

The Reitbrook dome is one of the best documented active salt domes in the world. It was first discovered in 1937. Since then, 265 wells have been drilled in the

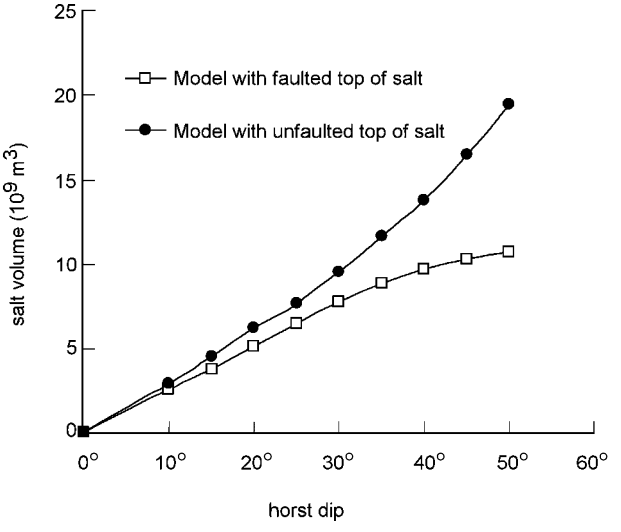

Figure 17. Dip of the horst and the volume of the dome for the faulted and unfaulted top of salt.

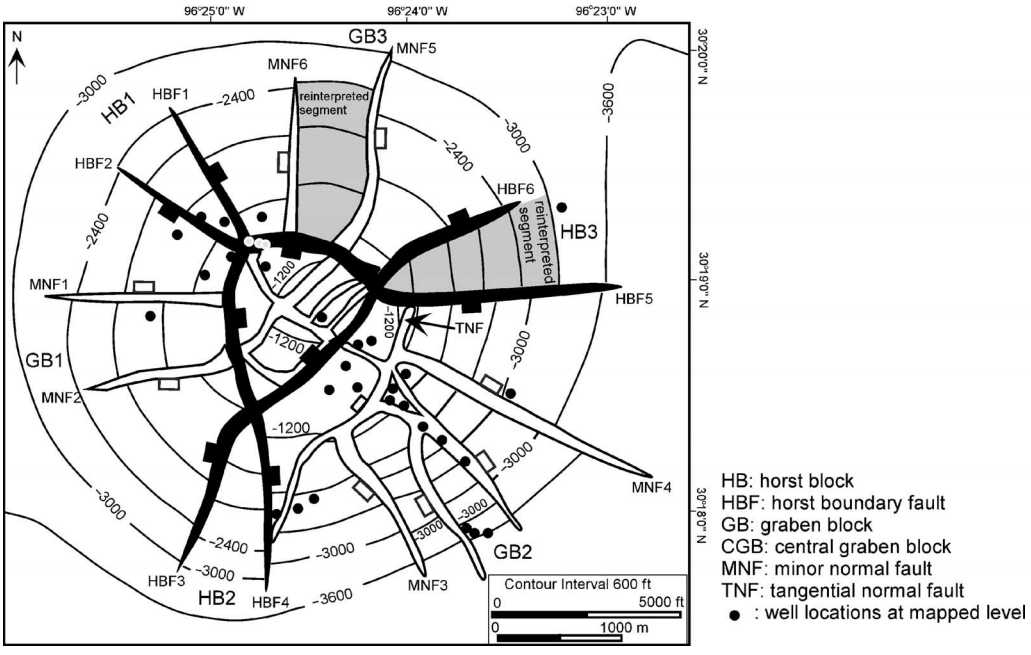

Figure 18. An alternative interpretation of the structure contour map of the Clay Creek dome drawn on top of the Wilcox Formation, based on results from the model. Compare to Figure 1a.

Reitbrook field. Early maps and cross sections were published by Behrmann (1949) and Gussow (1968). A recent detailed structural analysis conducted by Schmitz and Flixeder (1993) resulted in the complete reinterpretation of the field shown here (Figure 1b). The Reitbrook dome has an asymmetrical Y pattern of faulting. Three master normal faults cut the Reitbrook dome into one horst block (HB, Figure 3d), one wedge-shaped central graben (GB, Figure 3d), and three half grabens (HGB1, HGB2, HGB3, Figure 3d). No minor normal faults occur in the horsts. Four radial minor normal faults developed in the half graben HGB2, and three developed in HGB3. No minor fault is observed in the half-graben block HGB1. The dip of the horst block HB is about 16°. The dip of the half-graben block HGB1 is about 12°, similar to the dip predicted for the model dome with the faulted top of salt. The coincidence of the dip and the absence of minor faults within the block imply that the fault between HB and HGB1 (fault 1, Figure 3d) offsets the top of the salt. The dip of the half-graben block HGB2 is about 14°, steeper than the dip predicted by the model dome and close to the dip of the horst block, which implies that the fault between HB and HGB2 (fault 2, Figure 3d) probably detaches on the top of the salt. As expected from the model dome having an unfaulted top of salt (Figure 11), flank grabens and half grabens develop radial minor normal faults. The number and the location of the minor faults in HGB2 are comparable to what we observed in GB2 of the Clay Creek dome (Figure 3c). The dip direction of the minor faults is not the same as predicted by the model with the unfaulted top of salt. This is probably caused by fault 1, which offsets the top of the salt. The half graben HGB3 develops several minor normal faults. Not enough information is available to compare HGB3 and its boundary fault (fault 3, Figure 3d) with the model domes. Based on the well control and the cross sections (Schmitz and Flixeder, 1993), fault 3 ends against fault 1 before it reaches the top of the salt.

Based on the above interpretation, a slight revision of the fault pattern on cross section CC′ across the Reitbrook (Figure 19a) will produce better kinematic compatibility. Fault 1 is extended to offset the top of the salt, which allows a constant thickness in the Lower Cretaceous strata to be maintained (Figure 19b). Constant thickness is a feature of cross sections cut along the radial direction in the model.

DISCUSSION

The salt in the diapirs investigated and modeled in this article only partially penetrates the overburden strata. Radial normal faults cross each other near the crest of the domes (Figure 3). In the Gulf of Mexico, it is common to find radial normal faults terminating against the flanks of a circular salt stock (e.g., Belle Isle salt dome, Figure 20). This is probably the result of erosion of the crestal part

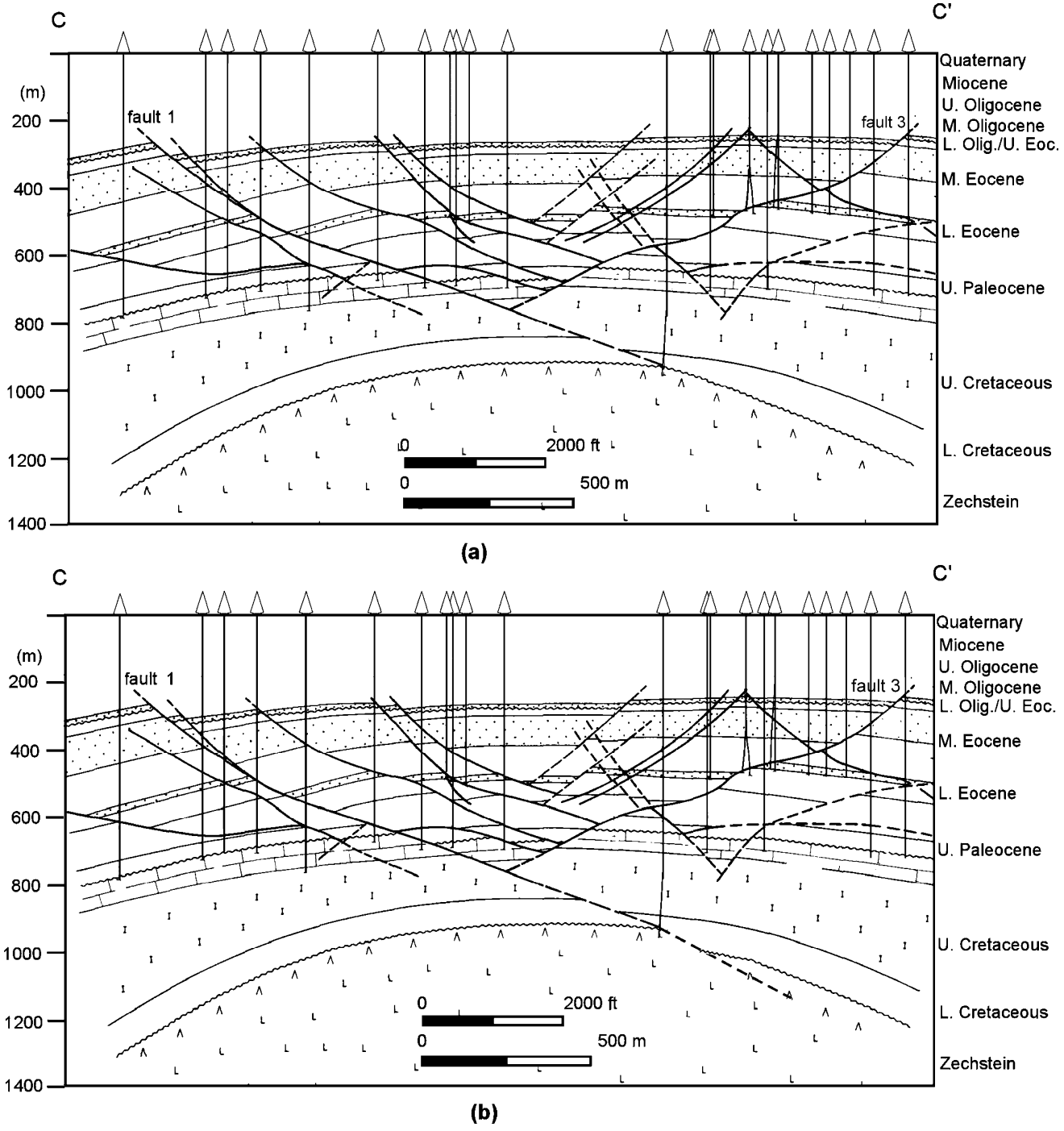

Figure 19. Revised interpretation of cross section CC′ across the center of the Reitbrook dome based on the result from the model dome. (a) Original cross section (from Schmitz and Flixeder, 1993, with kind permission of Springer Science and Business Media). For the location of the section, see Figure 6d. (b) Revised interpretation of the cross section.

of an active diapir with preservation of the radial fault pattern on the flanks. Radial faults that initiated in the active stage may remain active as long as the dip of bedding on the flanks continues to increase, even if the salt has reached the surface in the center (Figures 20a, b). During totally passive diapirism, bedding does not rotate significantly, and few faults exist (Figure 20a, c).

Master faults of an active dome may penetrate the salt or detach on the top of the salt. This has a large impact on the hanging-wall deformation and, thus, may

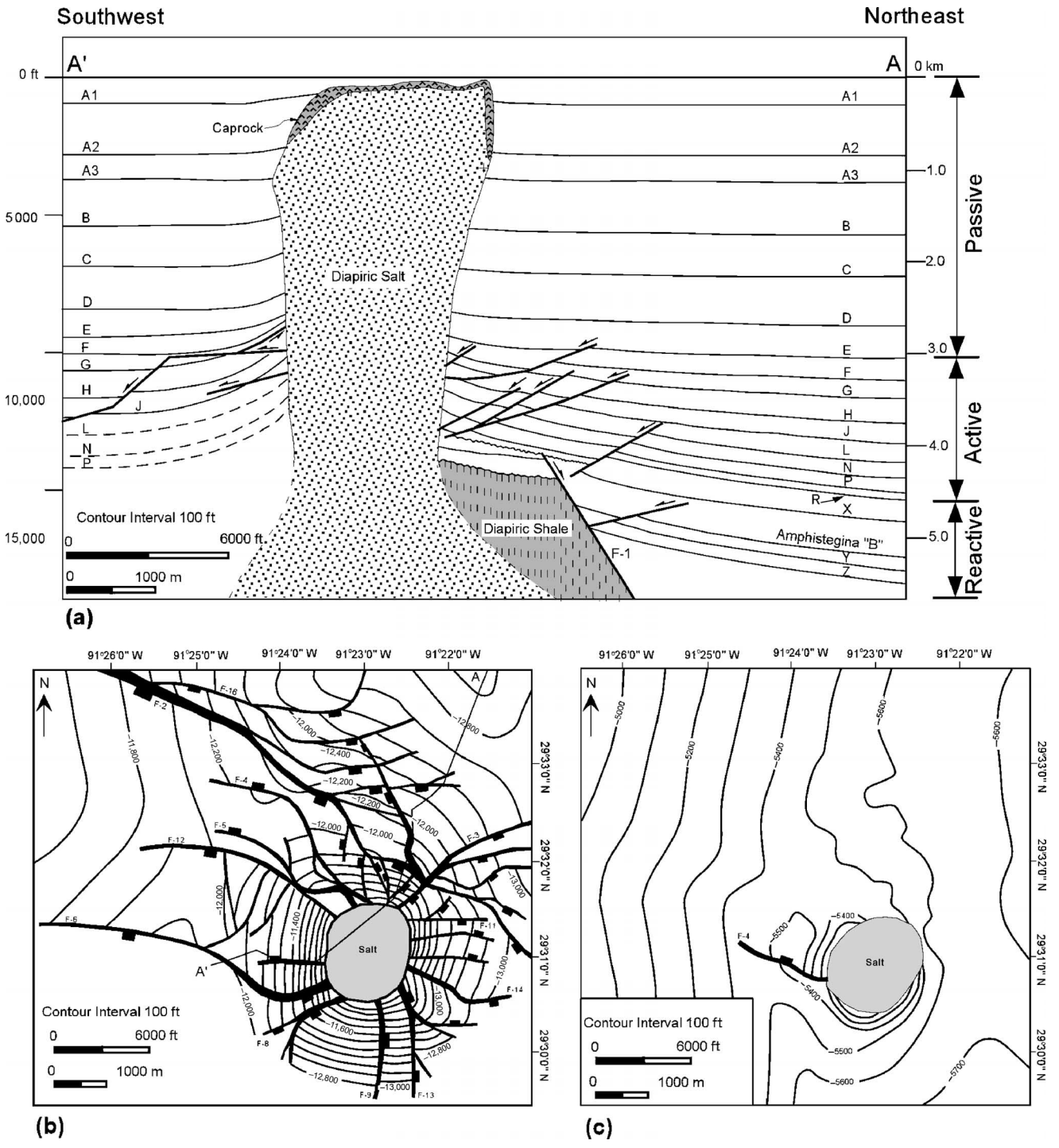

Figure 20. Belle Isle salt dome, Louisiana (modified from O'Neill, 1973). (a) Cross section (letters A1–Z represent the stratigraphic unit boundaries). Location given in (b). (b) Structure contour map drawn on the J horizon. (c) Structure contour map drawn on the B horizon.

have an impact on the quality of reservoirs. Master faults that cut the salt can grow without the formation of rollovers or new faults, whereas master faults that detach on the salt top lead to a greater chance of fractures and small-scale to subseismic faults in the hanging wall. As a result, reservoirs associated with faults detached on salt might be more compartmentalized and have multiple hydrocarbon contacts.

It has been suggested that the faults of the Clay Creek dome result from substratal solution collapse, not

arching of the overburden. Based on physical experiments, McDowell (1951) discarded this alternative and associated the radial fault pattern with the arching of the overburden strata. Since then, a number of studies have documented the structural style associated with solution collapse. Substratal solution-collapse features can occur without obvious faulting (Parker, 1967; Smith and Pullen, 1967; Jenyon, 1986; Gerhard et al., 1991). Where collapse faults occur, they are circumferential and either vertical (Christiansen, 1971; Gendzwill and Hajnal, 1971) or high-angle reverse with the classic upthrust shape (Nely, 1989; Ge and Jackson, 1998) that is so well known in association with vertical block displacements (e.g., Sanford, 1959; Logan et al., 1978). This evidence clearly indicates that radial normal faults are caused by extension over the crest of the dome, not vertical subsidence of the dome. Salt dissolution and collapse may, however, further complicate the radial fault pattern of active salt domes, e.g., increasing the displacement of individual faults or creating more faults in the overburden strata. The kinematic models presented here have not considered salt dissolution, and so we should be cautious when applying the model to domes with substantial salt dissolution and collapse.

It is common in the published literature to see the style of a dome characterized with a single cross section as having, for example, a central graben, a half graben, or a central horst. We have shown that the apparent structural style can be very different in cross sections in different locations across a single dome. A single X-pattern dome may appear to have either a central graben or a central horst. Both X and Y dome styles are highly asymmetrical in master-fault-perpendicular sections, but symmetrical in master-fault-parallel sections. The structures in the perpendicular sections are more complicated and variable than those on parallel sections. A true central graben (Y-pattern dome) will be highly deformed and show unrestorable structural thinning because of out-of-plane volume transport.

CONCLUSIONS

1. Field examples of gently arched, active circular domes suggest that faulting initiates with either two (X pattern) or three (Y pattern) throughgoing master faults. Both patterns are shown here to be kinematically viable, which means that the dome can grow by fault slip and block rotation without losing continuity across the faults and without requiring new major faults. The master faults become mutually offsetting with increasing displacement. The Y pattern develops a highly deformed central graben.
2. Master faults that detach on the top of the salt require a rollover in the hanging wall, which is likely to be manifested as one or more antithetic minor faults parallel to the master fault. This is the most significant alteration of the initial fault pattern necessary to maintain kinematic compatibility of the fault network. Master faults that cut the salt can grow without the formation of rollovers or new faults.
3. The apparent structural style of a dome in cross section may change significantly depending on the location and orientation of the profile.
4. The initial fault pattern influences the piercement efficiency. Given the same rate of salt injection and the same number of master faults, an active dome with faults offsetting the top of the salt grows more rapidly than a dome with a smooth top and, hence, is more likely to develop into a piercement structure.
5. As examples of using kinematically compatible models to aid in interpretation, we suggest changes to the fault patterns of both the Clay Creek and Reitbrook domes that will make them more internally consistent. The Clay Creek fault pattern can be improved by changing the dip direction of one of the minor faults from synthetic to antithetic and by changing the connectivity along one master fault. The fault pattern of the Reitbrook dome implies that one of the three master faults cuts the salt, although the other two do not. We suggest that the kinematically compatible models presented here can serve as a guide to interpreting fault patterns in other active domes where imaging may be imperfect or fault correlations may be open to question.

REFERENCES CITED

Barton, D. C., 1933, Mechanics of formation of salt domes with special reference to Gulf Coast salt domes of Texas and Louisiana: AAPG Bulletin, v. 17, p. 1025–1083.

Behrmann, R. B., 1949, Geologie und lagerstatte des Oelfeldes Reitbrook bei Hamburg, *in* A. Bentz, eds., Erdoel und tektonik in Nordeswestdeutschland: Hannover, Sammelband, p. 190–221.

Braunstein, J., and G. D. O'Brien, eds., 1968, Diapirism and diapirs: AAPG Memoir 8, 444 p.

Brewer, R. C., and R. H. Groshong, Jr., 1993, Restoration of cross sections above intrusive salt domes: AAPG Bulletin, v. 77, p. 1769–1780.

Christiansen, E. A., 1971, Geology of the Crater Lake collapse structure in southeastern Saskatchewan: Canadian Journal of Earth Science, v. 8, p. 1505–1513.

Clark, J. A., J. A. Cartwright, and S. A. Stewart, 1999, Mesozoic

dissolution tectonics on the West Central Shelf, UK Central North Sea: Marine and Petroleum Geology, v. 16, p. 283–300.
Cloos, E., 1955, Experimental analysis of fracture patterns: Geological Society of America Bulletin, v. 66, p. 241–256.
Davis, D., and E. Lambert, 1963, Mesozoic–Paleozoic producing areas of Mississippi and Alabama: Jackson, Mississippi, Mississippi Geological Society, v. 2, unnumbered.
Davison, I., I. Alsop, and D. Blundell, 1996, Salt tectonics: Some aspects of deformation mechanics, *in* G. I. Alsop, D. J. Blundell, and I. Davison, eds., Salt tectonics: Geological Society (London) Special Publication 100, p. 1–10.
Davison, I., I. Alsop, P. Birch, C. Elders, N. Evans, H. Nicholson, P. Rorison, D. Wade, J. Woodward, and M. Young, 2000a, Geometry and late-stage structural evolution of Central Graben salt diapirs, North Sea: Marine and Petroleum Geology, v. 17, p. 499–522.
Davison, I., I. Alsop, N. G. Evans, and M. Safaricz, 2000b, Overburden deformation patterns and mechanisms of salt diapir penetration in the Central Graben, North Sea: Marine and Petroleum Geology, v. 17, p. 601–618.
Eisenberg, R. A., and M. Dixon, 1999, Application of visualization technologies for interpretation and prospect assessment, Main Pass 299 Gulf of Mexico (abs.): AAPG Annual Meeting Program, v. 8, p. A37–A38.
Ewing, T. E., 1986, Structural styles of the Wilcox and Erio growth-fault trends in Texas: Constraints on geopressured reservoirs: Bureau of Economic Geology, University of Texas at Austin, Report of Investigations 154, 86 p.
Fails, T. G., 1990, Variation in salt dome faulting, Coast Salt Basin: Gulf Coast Association of Geological Societies Transactions, v. 40, p. 181–193.
Ferguson, W. B., and J. W. Minton, 1936, Clay Creek salt dome, Washington County, Texas: AAPG Bulletin, v. 20, p. 68–90.
Ge, H., and M. P. A. Jackson, 1998, Physical modeling of structures formed by salt withdrawal: Implications for deformation caused by salt dissolution: AAPG Bulletin, v. 82, p. 228–250.
Gendzwill, D. J., and Z. Hajnal, 1971, Seismic investigation of the Crater Lake collapse structure in southeastern Saskatchewan: Canadian Journal of Earth Science, v. 8, p. 1514–1524.
Gerhard, L. C., S. B. Anderson, and D. W. Fischer, 1991, Petroleum geology of the Williston Basin, *in* M. W. Leighton, D. R. Kolata, D. F. Oltz, and J. J. Eidel, eds., Interior cratonic basins: AAPG Memoir 51, p. 507–559.
Grinstead, F. A., 1962, Sugarland field, Fort Bend County, Texas, *in* R. L. Denham, eds., Typical oil and gas fields of southeast Texas: Houston Geological Society, p. 219–220.
Groshong, R. H. Jr., 1988, Low-temperature deformation mechanisms and their interpretation: Geological Society of America Bulletin, v. 100, p. 1329–1360.
Groshong, R. H. Jr., 1990, Unique determination of normal fault shape from hangingwall bed geometry in detached half grabens: Eclogae Geologicae Helvetiae, v. 83, p. 455–471.
Groshong, R. H. Jr., 2006, 3-D structural geology, 2d ed.: Heidelberg, Springer-Verlag, 400 p.
Gussow, W. C., 1968, Salt diapirism: Importance of temperature, and energy source of emplacement, *in* J. Braunstein and G. D. O'Brien, Diapirism and Diapirs: AAPG Memoir 8, p. 16–52.
Halbouty, M. T., 1967, Salt domes, Gulf region, United States and Mexico: Houston, Gulf Publication Company, 425 p.
Health, F. E., J. A. Waters, and W. B. Ferguson, 1931, Clay Creek dome, Washington County, Texas: AAPG Bulletin, v. 15, p. 247–256.
Hossack, J., 1995, Geometric rules of section balancing for salt structures, *in* M. P. A. Jackson, D. G. Roberts, and S. Snelson, eds., Salt tectonics: A global perspective: AAPG Memoir 65, p. 29–40.
Jackson, M. P. A., and C. J. Talbot, 1991, A glossary of salt tectonics: Texas, Bureau of Economic Geology Geological Circular 91-4, 44 p.
Jackson, M. P. A., and B. C. Vendeville, 1994, Regional extension as a geologic trigger for salt diapirism: Geological Society of America Bulletin, v. 106, p. 57–73.
Jackson, M. P. A., C. J. Talbot, and R. R. Cornelius, 1988, Centrifuge modeling of the effects of aggradation and progradation on syndepositional salt structures: Texas, Bureau of Economic Geology Geological Circular 173, 93 p.
Jenyon, M. K., 1986, Salt tectonics: New York, Elsevier Applied Science Publishers, 191 p.
Johnston, D. H., J. J. Shyeh, and J. E. Eastwood, 2001, Interpretation and modeling of time-lapse seismic data: Lena field, Gulf of Mexico: Joint Houston Geological Society/Geophysical Society of Houston dinner meeting, March 2001: http://www.hgs.org/meet0301.htm (accessed July 20, 2003).
Karges, H. E., 1975, Mississippi shallow salt domes: Gulf Coast Association of Geological Societies and SEPM (Gulf Coast) meeting, p. 1726.
Lat-Long Services, 2006, Look up the exact location of millions of places: http://www.lat-long.com (accessed September 8, 2006).
Link, T. A., 1930, Experiments relating to salt-dome structures: AAPG Bulletin, v. 14, p. 483–508.
Logan, J. M., M. Friedman, and M. T. Stearns, 1978, Experimental folding of rocks under confining pressure: Pt. VI. Further studies of faulted drape folds: Geological Society of America Memoir 151, p. 79–99.
Looff, K. M., and K. M. Looff, 1999, Possible geologic influence on salt falls associated with the storage caverns at Bryan Mound, Brazoria County, Texas: Gulf Coast Association of Geological Societies Transactions, v. 49, p. 322–331.
McDowell, A. N., 1951, The origin of the structural depression above Gulf Coast salt domes with particular reference to Clay Creek dome, Washington County, Texas: M.S. thesis, Texas A&M University, College Station, Texas, 26 p.
Nelson, T. H., 1991, Salt tectonics and listric-normal faulting, *in* A. Salvador, eds., The Gulf of Mexico basin: Geological Society of America, The Geology of North America, v. J, p. 73–89.
Nely, G., 1989, Les seriés a évaporite en exploration pétrolié, 2 méthodes géophysiques: Paris, Editions Technip, 259 p.
Nettleton, L. L., 1934, Fluid mechanics of salt domes: AAPG Bulletin, v. 18, p. 1175–1204.
Nettleton, L. L., 1943, Recent experimental and geophysical evidence of mechanics of salt-dome formation: AAPG Bulletin, v. 27, p. 51–63.
O'Neill, C. A., 1973, Evolution of Belle Isle salt dome, Louisiana: Gulf Coast Association of Geological Societies Transactions, v. 23, p. 115–135.
Parker, J. M., 1967, Salt solution and subsidence structures, Wyoming, North Dakota, and Montana: AAPG Bulletin, v. 51, p. 1929–1947.
Parker, T. J., and A. N. McDowell, 1951, Scale model as guide to interpretation of salt dome faulting: AAPG Bulletin, v. 35, p. 2076–2086.
Parker, T. J., and A. N. McDowell, 1955, Model studies of salt-dome tectonics: AAPG Bulletin, v. 39, p. 2384–2470.
Rowan, M. G., and R. Kligfield, 1989, Cross section restoration and balancing as an aid to seismic interpretation in extensional terranes: AAPG Bulletin, v. 73, p. 955–966.
Rowan, M. G., T. F. Lawton, K. A. Giles, and R. A. Ratliff, 2003, Near-salt deformation in La Popa Basin, Mexico, and the northern Gulf of Mexico: A general model for passive diapirism: AAPG Bulletin, v. 87, p. 733–756.
Sanford, A. R., 1959, Analytical and experimental study of simple geologic structures: Geological Society of America Bulletin, v. 70, p. 19–52.

Schmitz, J., and F. Flixeder, 1993, Structure of a classic chalk oil field and production enhancement by horizontal drilling, Reitbrook, NW Germany, *in* A. M. Spencer, eds., Generation, accumulation and production of Europe's hydrocarbons III: European Association of Petroleum Geoscientists Special Publication 3, p. 144–154.

Schultz-Ela, D. D., M. P. A. Jackson, and B. C. Vendeville, 1993, Mechanics of active salt diapirism: Tectonophysics, v. 228, p. 275–312.

Smith, D. A., and F. A. E. Reeve, 1970, Salt piercement in shallow Gulf Coast salt structures: AAPG Bulletin, v. 54, p. 1271–1289.

Smith, D. G., and J. R. Pullen, 1967, Hummingbird structure of southeast Saskatchewan: Bulletin of Canadian Petroleum Geology, v. 15, p. 468–482.

Smith, S. W., et al., 1988, Tiger Shoal field, offshore Louisiana, *in* J. R. J. Studlick, J. G. Bryant, J. A. Hartman, and R. D. Shew, eds., New Orleans Geological Society, offshore Louisiana oil & gas fields: v. 2, p. 173–178.

Tang, L., C. Jia, Z. Jin, S. Chen, X. Pi, and H. Xie, 2004, Salt tectonic evolution and hydrocarbon accumulation of Kuqa foreland fold belt, Tarim Basin, NW China: Journal of Petroleum Science and Engineering, v. 41, p. 97–108.

Turner, J. R., C. E. Gray, and N. B. Pollard, 2001, Resurgence of salt dome exploration in the Gulf Coast Mesozoic basins in Texas, Louisiana, and Mississippi: Gulf Coast Association of Geological Societies Transactions, v. 51, p. 305–312.

Vendeville, B. C., and M. P. A. Jackson, 1992, The rise of diapirs during thin-skinned extension: Marine and Petroleum Geology, v. 9, p. 331–353.

Volozh, Y., C. Talbot, and A. Ismail-Zadeh, 2003, Salt structures and hydrocarbons in the Pricaspian Basin: AAPG Bulletin, v. 82, p. 313–334.

Waguespack, S. J., ed., 1983, Salt domes of south Louisiana, v. 3: New Orleans Geological Society, 142 p.

White, N. J., J. A. Jackson, and D. P. McKenzie, 1986, The relationship between the geometry of normal faults and that of the sedimentary layers in their hangingwalls: Journal of Structural Geology, v. 8, p. 897–909.

Withjack, M., 1979, An analytical model of continental rift fault patterns: Tectonophysics, v. 59, p. 59–81.

Withjack, M., and C. Scheiner, 1982, Fault patterns associated with domes: An experimental and analytical study: AAPG Bulletin, v. 66, p. 302–316.

Yin, H., 2003, Structural interpretation and validation of three-dimensional piercement structures: Ph.D. dissertation, University of Alabama, Tuscaloosa, Alabama, 150 p.

Yin, H., and R. H. Groshong, Jr., 2003, Geometric properties of active piercement structures: Geologic insight from 3-D kinematic models: Gulf Coast Association of Geological Societies Transactions, v. 53, p. 887–899.

Yin, H., and R. H. Groshong, Jr., 2006, Balancing and restoration of piercement structures: Geologic insights from 3D kinematic models: Journal of Structural Geology, v. 29, p. 99–114.